Three-Dimensional Electrospun Micropatterned Cellulose Acetate Nanofiber Surfaces with Tunable Wettability

Manohar Kakunuri[ϒ*], Nandula D. Wanasekara[!], Chandra S. Sharma[ϔ], Mudrika Khandelwal[ϒ], Stephen J. Eichhorn[!]

[ϒ]Department of Material Science and Metallurgical Engineering and [ϔ]Department of Chemical Engineering, Indian Institute of Technology Hyderabad, Kandi, Telangana 502285, India.

[!]College of Engineering, Mathematics and Physical Sciences, University of Exeter, Exeter, Devon, EX4 4QF, United Kingdom.

Correspondence to: Manohar Kakunuri (Email*: manohar@iith.ac.in*)

((Additional Supporting Information may be found in the online version of this article.))

ABSTRACT

Three-dimensional polymer nanofibrous mats with tunable wettability have been fabricated using a single step non-conductive template assisted electrospinning process. Cellulose acetate nanofibers are electrospun over a nylon mesh, which acts as the template. The as-deposited fiber mat is removed from this template to produce a free standing three-dimensional micropatterned nanofibrous mat. By simply varying the template mesh dimensions, the fraction of the air-liquid interface can be changed which allows control of the wetting mechanics. It is shown that the water contact angle can be varied from about 30 ^{o} for a planar network to about 140 ^{o} for a patterned mat implying a complete transition from hydrophilic to hydrophobic behaviour. Furthermore, upon stretching the fiber mat loses its pattern irreversibly and reducing the contact angle from 140 ^{o} to 110 ^{o} with increasing stretching.

Keywords: electrospinning; hydrophobic fiber mat; patterned nanofabric; template assisted patterning

INTRODUCTION:

Several applications have been reported for micropatterned nanofibrous mats, including scaffolds for tissue engineering, Microelectromechanical systems (MEMS) and for creating surfaces with tunable wettability.[1–3] Micropatterning is useful for enhancing hydrophobicity specifically, since it is difficult to obtain contact angles greater than 120 ^{o} for planar surfaces by normal methods such as low surface energy coatings.[4] Microfabrication is used to fabricate

superhydrophobic micropatterned surfaces, where the surface topographies are inspired from nature *e.g.* the papillae structure of the lotus leaf.[5]

In most previous studies, hydrophobic and superhydrophobic surfaces have been fabricated by a two-step procedure.[5–9] Different microfabrication techniques such as etching, lithography or bio-mimicking were first used to fabricate hierarchical surface topographies, which were then coated with low surface energy materials such as fluoroalkylsilanes, silicone compounds, and wax.[5–9]

Among an array of approaches to enhance surface roughness for contact angle control, electrospinning has gained special attention due to its ease of operation, control and scalability.[11] Various polymers and their composite derived electrospun nanofibrous mats have been used for preparing superhydrophobic surfaces.[10] It has been shown that the hydrophobicity of electrospun nanofibrous mats can be further enhanced by increasing surface roughness by introducing porosity, embedding nanoparticles, or by template-based extrusion and by micropatterning using photolithography.[2,3,11] However, photolithography based patterning and template-based extrusion are multi-step processes and are limited by scalability.

It is also known from the Wenzel and Cassie-Baxter classical wettability models, that, simply increasing the surface roughness cannot convert a hydrophilic surface into a hydrophobic surface.[12,13] The Wenzel model states that for hydrophilic surfaces, the contact angle decreases (hydrophilicity increases) with an increase in roughness.[13] However, by designing a nanofibrous micropatterned surface with a composite solid-liquid-air interface, with trapped air in the cavities of the patterned surface, one can achieve a hydrophilic to hydrophobic transition. According to the Cassie-Baxter theory, a hydrophilic to hydrophobic transition can occur at a

high air-liquid interface fraction and this transition also depends on the contact angle of the flat surface of the same material.[13] In addition to surface roughness, air trapped between elements of the rough surface also play a key role in controlling the wettability of the surfaces.[14] Capillary pressure (non-wetting pressure) due to trapped air decreases with increasing distance between the elements and with an increasing feature size. Further, micropatterned samples with non-communicating air gaps show robust hydrophobicity. This contrasts with micropatterned surfaces with communicating air gaps which tend to allow air to escape reducing hydrophobicity over time. [14] Optimizing the surface design of materials with non-communicating air gaps is therefore desired for fabricating robust hydrophobic surfaces.

Fabrication of micropatterned electrospun nanofibrous surfaces, for the formation of composite interfaces, requires a good control on the nanofiber deposition. Selective deposition of the fibers as the jet is drawn away from the tip of the syringe is difficult as it undergoes bending instabilities and whipping due to the applied high electric field.[15] However, to overcome this, methods such as near-field electrospinning, parallel-plate electrospinning and magnetic field assisted electrospinning have been used to preferentially align electrospun fibers in selected areas.[16–19] Further, for large area patterning, electro-conductive templates have been used to obtain preferential deposition.[20–22] This approach has enabled nanofibers to be preferentially directed towards the protrusions of a conductive template since they possess higher charge density. Alternatively, patterned fibrous mats have also been fabricated using easily available non-conductive templates and by placing a thin layer of non-conductive material over a conductive and patterned surface.[23–25]

Recently, Zhang *et al.* have studied the influence of insulating templates on electrospun nanofibrous mats.[23] The deposition of the fibers was found to depend on the opening size of the templates.[23] It was observed that for a template with an opening diameter of 2 mm, fibers were deposited in the open area over the aluminum foil, due to greater attraction of charged jets towards the conductive substrate. Interestingly, for templates with smaller opening diameters (1.5 mm and 0.9 mm), the fibers were preferentially deposited over the protrusions of the non-conductive template. This was attributed to the attraction of charged jets towards the non-conductive mesh, polarized and charged under the strong electric field.[23] However, the reported nanofibrous mats possessed features with large dimensions (opening diameters more than 0.9 mm), and no wettability studies were reported.

In this paper, we report the use of nylon meshed templates with opening sizes of 50 to 200 μm. Hydrophilic cellulose acetate (CA) is used as the polymer precursor for the electrospun fibers. The CA nanofibers are hydrophilic in nature and their wettability has been previously altered by grafting low surface energy functional groups.[6,26] We have alternatively tuned the wettability of the electrospun CA nanofibrous mats by engineering the solid-liquid-air interface and capillary pressure, simply by varying the template mesh opening size. Large area (~10 cm × 10 cm) three dimensional micropatterned nanofibrous mats were prepared in this study which can be easily peeled off from the template to make a free standing fabric. Several applications such as drug delivery, tissue scaffolding, oil-water separation, selective permeability membranes can be envisaged for the produced fabric.

EXPERIMENTAL SECTION:

Materials and Methods. CA (molecular weight 29000) was purchased from Sigma Aldrich, UK, N, N-dimethylacetamide and acetone were purchased from Merck Specialties Private Limited, India. Nylon meshes with various mesh opening sizes were purchased from Plastok, UK. A 16% (w/v) CA solution was prepared by mixing cellulose acetate powder in a 2:1 (v/v) ratio with a mixed solvent system (N,N-dimethylacetamide and acetone) and was then stirred, at room temperature, until a clear solution was obtained.

Table 1. Specifications of meshes used as a template for 3D patterning.

Mesh Opening (µm)	Open area fraction	Diameter of the wire (µm)	Thickness (µm)
50	0.37	33	50
100	0.44	48	80
200	0.48	80	185

The electrospinning setup used in this study was essentially the same as a conventional configuration, except a dielectric nylon mesh of size 10 cm × 10 cm was placed on the aluminum current collector as shown in Figure 1. The as-prepared CA solution was filled into a syringe with a 18 gauge needle and then electrospun onto the nylon meshes. Nylon meshes with opening sizes of 50, 100 and 200 µm were used which correspond to open area fractions of 0.37, 0.44 and 0.48 respectively. Detailed mesh specifications are described in Table 1. During the deposition, a field of 2 kV/cm and a flow rate of 10 µl/min was maintained. After 20

min of deposition, fiber mats were separated from the nylon mesh and the surface in contact with the mesh was further characterized.

Samples are denoted as bm-x in subsequent sections, where 'bm' corresponds to bottom surface (fiber mat surface in contact with the mesh before peeling) and x corresponds to the mesh opening size in µm.

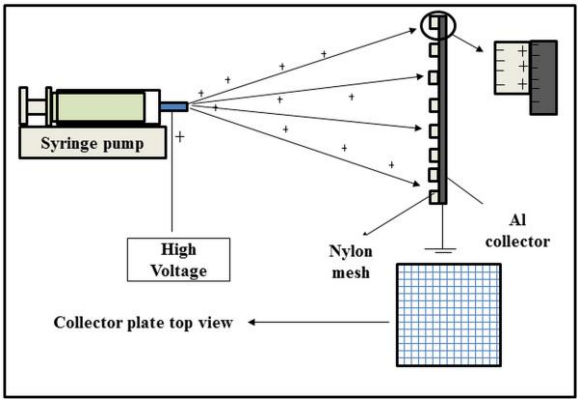

Figure 1. Schematic of the electrospinning setup used for the production of the three dimensional micropatterned nanofabric surfaces

Characterization. The surface topography of the patterned nanofibrous was examined using a three dimensional contact profiler (AEP Technology, USA; Model: Nanomap D). A low load (0.0029 mN) was used on the tip to prevent fiber damage during the scan. High resolution images of the samples were obtained using a desktop scanning electron microscope (SEM, Phenom World; Model: ProX). The wettability of the patterned and non-patterned fibrous mats collected over aluminum foil were studied using a sessile drop method with a goniometer (Rame-Hart, USA; Model: 290-F4); A 3 µl deionized (DI) water droplet ~2 mm diameter at room temperature was used for contact angle measurements. Contact angle experiments were

carried out in a dust free environment at 25 ^{o}C. Contact angle values for the water droplets were measured on 3 different samples. The contact angle values vary by ±3^{o} from sample to sample. Contact angle values mentioned in this report correspond to the water droplet image shown in the figures and the standard deviation was calculated for the 20 measurements with a time interval of 1 sec on the same sample.

RESULTS AND DISCUSSION

Fabrication of micropatterned nanofibrous mats

An SEM image of a 50 µm nylon mesh used as one of the templates for fabricating the three dimensional CA nanofiber mats is shown in Figure 2a. Nylon meshes were attached to an aluminum collector using double-sided tape at the corners to avoid electric field distortion due to the air gap.[24] Figure 2b shows the side of the mesh facing the collector after deposition.

In general, it is the electrostatic forces formed between the charged jet and the conductive collector that control the deposition of fibers. When a non-conductive material such as nylon is introduced into an electric field, it is found to disrupt the electric field by reducing the electrostatic interaction between the oppositely charged aluminum collector and the electrospinning jet.[23] Further, nylon as a material can be polarized under a strong electric field leading to the generation of negative static charges by static induction and polarization. This results in the attraction of the positively charged jet towards the mesh. This mechanism forms patterned fibers on the surface of the nylon mesh as shown in Figure 2c.

The electrospinning time also influences the deposition and therefore the fiber patterns. To better understand this, we have studied the morphologies of fiber mats deposited after 10 min and 20 min. Initially, positively charged fibers are attracted towards the polarized nylon surface

protrusions and form three dimensional architectures as illustrated in Figure 2d. On continuing the deposition further, the spinning jet experiences a repulsion from the fibers deposited over the mesh, and this randomizes their deposition. An extended deposition of ~20 min results in the disappearance of a pattern on the side opposite to that in contact with the mesh as shown in Figure 2e. Further, we also measured the fiber deposition density in terms of area coverage (fraction of fibers in a given area) and also the number of fibers per unit area using ImageJ software from high magnification SEM images (Figure S1). Fiber density (77% coverage; 65 fibers per 100 μm^2) near the nylon mesh line was found to be larger compared to around the mesh openings (28% coverage; 30 fibers per 100 μm^2).

The small opening size of meshes used in this work prevent fiber deposition onto the aluminum collector directly. Instead, the nanofibres tend to suspend over the mesh openings, which also helps with the separation of the electrospun mat from the collector. Additionally, the effect of the mesh opening size on the fiber diameter distribution was investigated. The diameter of 100 individual fibers was measured using Fiber Matrix software. Fiber diameter distributions are reported as Supporting Information for fibers deposited over 50 and 200 µm openings respectively (Figure S2). There was no significant change in the fiber diameter distribution for both cases; fiber diameter varies in the same range from 150 to 600 nm.

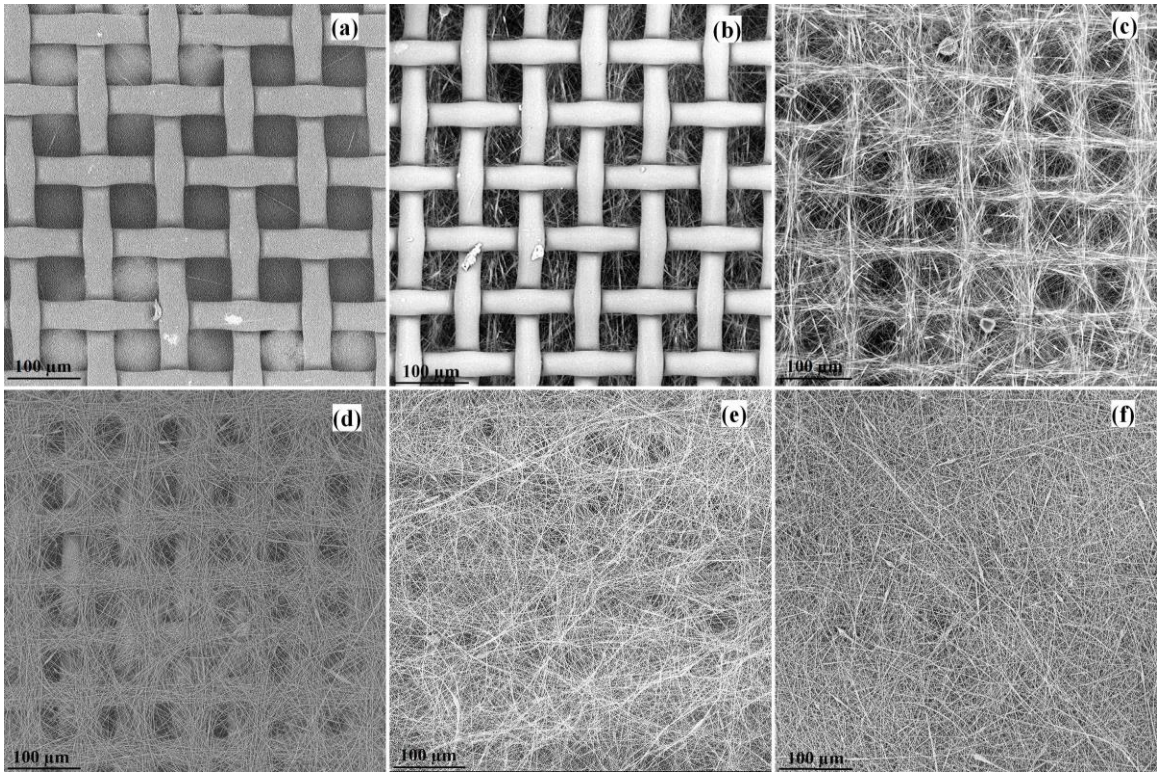

Figure 2. Typical SEM images of the (a) nylon mesh with an opening size of 50 µm, (b) surface of the nylon mesh (in contact with the Al collector) after removing from the collector, (c) patterned surface after removing from the collector and the mesh (surface in contact with the mesh), (d) syringe side view of the fiber mat after 10 min of deposition and (e) the syringe side view of the fiber mat after a 20 min deposition time; (f) a random fiber mat deposited over the Al foil.

Figure 3a shows the topography of the nanofibrous mat prepared using a 50 µm opening size nylon mesh after 20 min deposition time. Thickness of the peeled fiber mat was measured to be ~18 µm using a digital Vernier caliper while the fiber density was calculated to be 0.152 g/cm^2. This fiber mat was placed on a flat glass slide and used as a sample for surface topography measurements. Using a 3D profile from Figure 3a (the black line shown), the depth of

patterning has been determined and found to be ~12 µm (Figure 3b). The image confirms the initial preferential deposition over the mesh and the random deposition obtained after prolonged electrospinning, which results in the formation of a cone-like cavity within the mesh opening area.

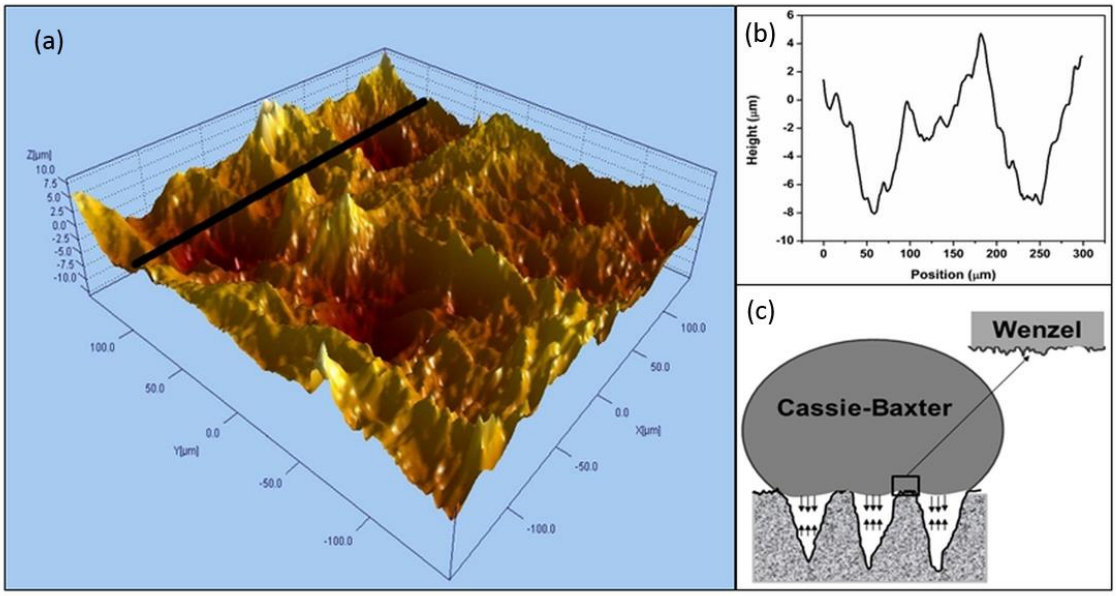

Figure 3. A typical (a) 3D profile of the bm-50 sample (XY is fiber deposition plane and Z is deposition thickness), and (b) a two dimensional profile of the bm-50 sample for the line of interest as shown in Figure a; the line corresponds to the bisector of a mesh opening (c) A schematic of the contact modes between a water droplet and a patterned structure.

The wettability of micropatterned fibrous mats, with cone-like cavities discussed above, was studied by measuring static contact angles using a sessile drop method. The study was carried out on microfibrous mats patterned by meshes of 3 different mesh openings. Figure 4a-c shows the SEM images of micropatterned surfaces produced with the nylon meshes of opening sizes

50, 100 and 200 µm, along with the corresponding contact angle measurement images. Figure 4d shows an SEM image of a non-patterned electrospun nanofibrous mat and the corresponding contact angle measurement image. It is noted that CA nanofibrous mats are hydrophilic with a contact angle of 30^{o} while the patterned CA nanofibrous mats exhibit hydrophobic behaviour. The contact angle decreases as the mesh opening size increases as shown in Figure 4.

The cone-like cavities in the mats lead to a composite interface, comprising of solid-liquid and air-liquid interface. In such surfaces, downward acting hydrostatic forces and an upward acting capillary pressure, as shown in Figure 3c, plays an important role. Additionally, hydrophobic behavior of these patterned surfaces can be attributed to the reduced contact energy between the apexes of the patterned fiber mat.[27]

Downward acting forces favor the Cassie-Baxter to Wenzel transition, while the upward acting capillary pressure prevents wetting at the solid-liquid interface.[27]The dominance of either of the forces is determined by the dimensions of the cavities. In micropatterned surfaces, a transition from a Cassie-Baxter non-wetting state to a Wenzel wetting state occurs at high hydrostatic pressure, where the water replaces the air trapped in the cavities, depending on the dimensions of the composite interface.[28]

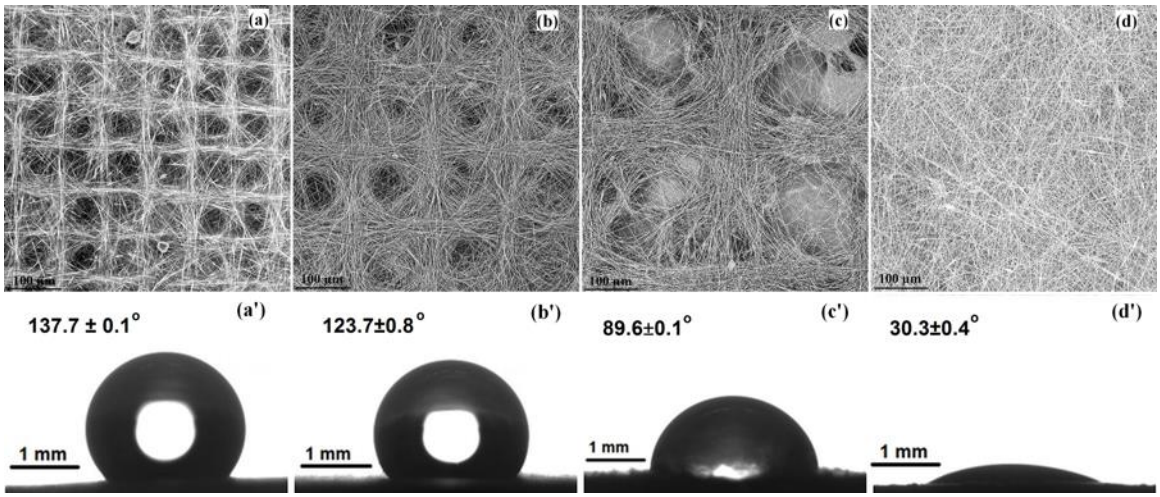

Figure 4. SEM images of (a) bm-50, (b) bm-100, (c) bm-200, (d) fiber mats and (a'), (b'), (c'), (d') are images of water droplets on samples (a), (b), (c), (d).

The magnitude of the forces acting on a water droplet sitting over a composite interface and its wettability behavior depends on the dimensions of the pattern, which plays a key role in changing the solid-liquid-air composite interfacial area and capillary pressure. Compared to planar fiber mats, patterned fiber mats with a notable air-liquid interface area fraction and capillary pressure show significantly higher contact angles.

Amongst the patterned mats, the sample with a low open area fraction (open area/solid area) (bm-50) of 0.37 as described in Table 1 shows the highest contact angle of 137.7 ± 0.1°, while a sample with the highest open area fraction (bm-200) of (0.48) exhibits the lowest contact angle of 89.6 ± 0.1 ° (Figure 3). This decrease in contact angle is attributed to a decreasing capillary pressure with increasing distance between the patterned grid lines and an excess deposition of fibers in the gaps due to an increase in the electrostatic attraction towards the aluminum target within the meshes as shown in Figure 4c. This deposition over the cone shaped cavities reduces

the size of the air pockets and also imparts some hydrophilicity to the surface. However, water droplets do not 'roll off' these micro patterned nanofibrous surfaces upon tilting due to the pinning effect of the hydrophilic cellulose acetate solid-liquid interface, as shown in Figure 3c.

Additionally, these patterned fiber mats were stretched to further understand the effect of the pattern on the wettability of the hydrophobic patterned mats. Stretching of the micropatterned nanofiber mats disrupts the patterning as shown in Fig. 5 (a-c). During this process the pattern was irreversibly removed from the networks, as shown in Figure 5. An increase in the stretch of the networks, stretching from 5% to 20%, resulted in a reduction in the water contact angle from 132 ^{o} to 116 ^{o}.

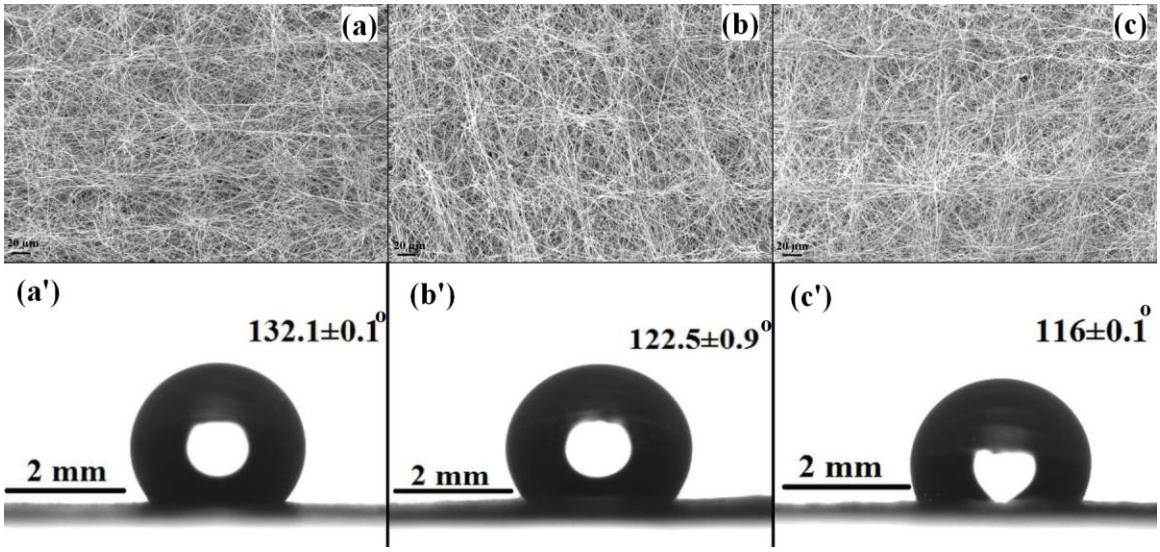

Figure 5. SEM images of a bm-50 sample after (a) 5%, (b) 10%, (c) 20% stretching and (a'), (b'), (c') are images of water droplet on samples (a), (b), (c).

The flexibility of our patterned fiber mats allows us to wrap them over curved surfaces. Figure 6 a shows the peeling of a patterned fiber mat from the mesh and Figure 6b shows an image of

a water droplet on a fiber mat wrapped around a cylindrical glass vial. It can be clearly seen that a water droplet has a high contact angle due to the hydrophobicity of the patterned fiber mat (bm-50); contact angle close to 140^{o}. Further, we also checked the wetting behavior with silicon oil and found that these fabrics are oleophilic. For practical use, these fabrics were also found not to sink when immersed in water due to their hydrophobicity and their porous nature.

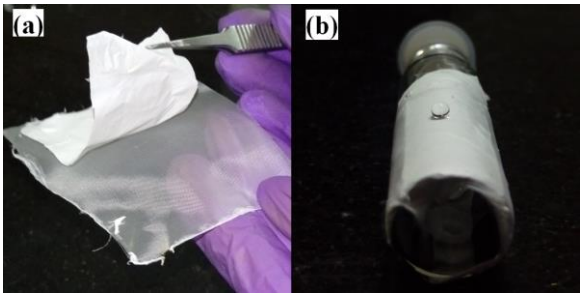

Figure 6. Digital images of (a) the peeling of a fiber mat from mesh, (b) water droplet sitting over a patterned fiber mat wrapped over a cylindrical glass vial

A single step method for the fabrication of three dimensional micropatterned nanofibrous mats with tunable wettability has been discussed. The proposed method could be extended to almost all polymers which can be electrospun, and to a wide variety of patterns. Such micropatterned three dimensional materials could be used for tissue engineering, controlled drug release and as a precursor to flexible electrode materials for supercapacitors and lithium ion batteries.[29-32] Further, tunable wettability makes such materials also suitable for making semipermeable membranes. A unique advantage of this method is the fabrication of fabrics with contrasting wettability on both sides of the mats.

CONCLUSIONS

Three dimensional micropatterned nanofibrous mats with tunable hydrophobicity have been produced in a single step templated electrospinning method. In the presence of a high electric field, the non-conducting template acquires surface charge due to polarization. The electrospun polymer jet is attracted to the charged template, producing a patterned surface. It has been shown that by simply changing the template mesh dimensions, the wettability of the standalone patterned fabric can be altered.

It has been shown that a non-patterned mat is hydrophilic whereas patterning induces hydrophobicity. The contact angle increased from ~89 ^{o} to ~138 ^{o} with a decrease in the template mesh opening dimension from 200 µm to 50 µm, due to increased upward thrust from the air pockets. Also as the mesh opening size increases, the influence of the charged template decreases, leading to a random deposition over the mesh opening and thus increasing the hydrophilic influence from the CA fibers. This simple approach enables large area fabrication of three dimensional patterned hydrophobic surfaces from hydrophilic materials.

ACKNOWLEDGMENT

MK acknowledges Dr. Ranjith Ramadurai and Ms. Mani Pujitha for their help in understanding electrostatic interactions of the dielectric material. Support of a DST-UKIERI grant is gratefully acknowledged. MK and CSS acknowledge the Indian Institute of Technology Hyderabad for providing necessary research infrastructure to carry out this work.

REFERENCES

1. Li, W-J., Tuli, R., Okafor, C., Derfoul, A., Danielson, K. G., Hall, D. J. and Taun, R. S. A *Biomaterials* **2005,** *26*, 599-609.
2. Sharma, C. S., Sharma, A. and Madou, M. *Langmuir* **2010**, *26*, 2218-2222.
3. Feng, L., Li, S., Li, H., Zhai, J., Song, Y., Jiang, L. and Zhu, D. *Angew. Chemie - Int. Ed*. **2002**, *41*, 1221-1223.
4. Blossey, R. *Nat. Mater.* **2003**, *2*, 301-306.
5. Bhushan, B., Jung, Y. C., Niemietz, A. and Koch, K. *Langmuir* **2009**, *25*, 1659-1666.
6. Ogawa, T., Ding, B., Sone, Y. and Shiratori, S. *Nanotechnology* **2007**, *18,* 165607.
7. Ma, M., Hill, R. M., Lowery, J. L., Fridrikh, S. V. and Rutledge, G. C. *Langmuir* **2005**, *21*, 5549-5554.
8. Oner, D. and Mccarthy, T. J. *Langmuir* **2000**, *16*, 7777-7782.
9. Tadanaga, K., Katata, N., Minami, T., *J. Am. Chem. Soc.* **1997,** *42*, 1996-1998.
10. Sas, I., Gorga, R. E., Joines, J.A. and Thoney, K. A. *J. Polym. Sci. Part B Polym. Phys*. **2012**, *50*, 824-845.
11. Ma, M., Gupta, M., Li, Z., Zhai, L., Gleason, K. K., Cohen R. E., Rubner M. F. and Rutledge G. C. *Adv. Mater*. **2007**, *19*, 255-259.
12. Jung, Y. C. and Bhushan, B. *Nanotechnology*, **2006,** *17*, 4970-4980.
13. Wenzel, R. N. *Ind. Engg. Chem.* **1936**, *28*, 988-994.
14. Dash, S., Alt, M. T. and Garimella, S. V. *Langmuir, **2012**, 28***,*** 9606-9615.
15. Reneker, D. H., Yarin, A. L., Fong, H. and Koombhongse, S. *J. Appl. Phys.* **2000,** *87*, 4531-4547.

16. Yang, D., Lu, B., Zhao, Y. and Jiang X. *Adv. Mater.***2007**, *19*, 3702-3706.

17. Bisht, G. S., Canton, G., Mirsepassi, A., Kulinsky, L., Oh, S., Dunn-Rankin, D. and Madou M. J. *Nano Lett.* **2011,** *11*, 1831-1837.

18. Li D., Wang, Y. and Xia, Y. *Nano lett.* **2003**, *3*, 1167-1171.

19. Zhou, F., Hubbard, P. L., Eichhorn, S. J. and Parker, G. J. M. *Polymer* **2011,** *52*, 3603-3610.

20. Ding, Z., Salim, A. and Ziaie, B. *Langmuir* **2009,** *25*, 9648-9652.

21. Wu, Y., Dong, Z., Wilson, S. and Clark, R. L. *Polymer* **2010,** *51***,** 3244-3248.

22. Zhang, D. and Chang, J.; *Adv. Mater.* **2007**, *19***,** 3662-3667.

23. Zhao, S., Zhou, Q., Long, Y.Z., Sun, G.H. and Zhang, Y. *Nanoscale* **2013,** *5,* 4993-5000.

24. Cho, S. J., Kim, B., An, T. and Lim, G. *Langmuir* **2010,** *26*, 14395-14399.

25. Dempsey, D. K., Schwartz, C. J., Ward, R. S., Iyer, A. V., Parakka, J. P. and Cosgriff-Hernandez, E. M. *Macromol. Mater. Eng.* **2010,** *295*, 990-994.

26. Ding, B., Li, C., Hotta, Y., Kim, J., Kuwaki, O. and Shiratori, S. *Nanotechnology*. **2006**, *17*, 4332-4339.

27. Gou, S., Mossman, M. and Whitehead, L. *Appl. Opt.* **2012,** *51*, 1645-1653.

28. Srinivasan, S., Chhatre, S. S., Gaurdado, J. O., Park, K. C., Parker A. R.; Rubner M. F., McKinley, G. H. and Cohen, R. E. *J. R. Soc. Interface* **2014,** *11*, 20140287.

29. Wang, C. and Wallace, G. G. *Electrochim. Acta* **2015**, *175*, 87-95.

30. Che, A.F., Germain, V., Cretin, M., Cornu D., Innocent C. and Tingry S. *New J. Chem*. **2011**, *35*, 2848-2853.

31. Wu, H., Hu, L., Rowell, M. W., Kong, D., Cha, J. J., McDonough, J. R., Zhu, J., Yang, Y., McGehee, M. D. and Cui, Y. *Nano Lett.* **2010**, *10*, 4242-4248.

32. Liu, Y., Zhou, J., Chen, L., Zhang, P., Fu, W., Zhao, H., Ma, Y., Pan, X., Zhang, Z., Han, W. and Xie, E. *ACS Appl. Mater. Interfaces*. **2015**, *7*, 23515-23520.

Table of content graphic